nature biotechnology

Engineered ascorbate peroxidase as a genetically encoded reporter for electron microscopy

Jeffrey D Martell[1], Thomas J Deerinck[2], Yasemin Sancak[3,4], Thomas L Poulos[5], Vamsi K Mootha[3,4], Gina E Sosinsky[2,6], Mark H Ellisman[2,6] & Alice Y Ting[1]

Electron microscopy (EM) is the standard method for imaging cellular structures with nanometer resolution, but existing genetic tags are inactive in most cellular compartments[1] or require light and can be difficult to use[2]. Here we report the development of 'APEX', a genetically encodable EM tag that is active in all cellular compartments and does not require light. APEX is a monomeric 28-kDa peroxidase that withstands strong EM fixation to give excellent ultrastructural preservation. We demonstrate the utility of APEX for high-resolution EM imaging of a variety of mammalian organelles and specific proteins using a simple and robust labeling procedure. We also fused APEX to the N or C terminus of the mitochondrial calcium uniporter (MCU), a recently identified channel whose topology is disputed[3,4]. These fusions give EM contrast exclusively in the mitochondrial matrix, suggesting that both the N and C termini of MCU face the matrix. Because APEX staining is not dependent on light activation, APEX should make EM imaging of any cellular protein straightforward, regardless of the size or thickness of the specimen.

Determining the localization of proteins using EM has been integral to elucidating many cellular processes. Antibody-based detection[5–8], the most common approach, requires either permeablizing treatments, which degrade cellular ultrastructure[9,10], or ultracryosectioning of sucrose-cryoprotected samples and immunostaining of each individual section[11]. Genetically encoded tags do not require permeabilization, technically demanding ultracryosectioning or staining of individual sections because they localize to the site of interest before fixation. But existing genetic tags for EM have limitations. Horseradish peroxidase (HRP) is a sensitive[12] genetically encoded tag that catalyzes the H_2O_2-dependent polymerization of 3,3′-diaminobenzidine (DAB) into a localized precipitate that gives EM contrast after treatment with OsO_4[13,14]. However, HRP is inactive when expressed in the mammalian cytosol[1], likely because its four structurally essential disulfide bonds and two Ca^{2+} binding sites do not form in reducing and Ca^{2+}-scarce environments. A genetically encoded tag called miniSOG[2] provides EM contrast in all cellular compartments by means of light-dependent generation of $^1O_2$, which produces a DAB precipitate, but the requirement for light can be limiting when large or thick samples need to be stained for EM. ReAsH is another light-dependent tag, but its nonspecific labeling and the challenge of probe delivery into tissue limit its utility[15,16].

A re-engineered version of HRP with activity in the cytosol would overcome the limitations of existing methods[17], but our attempts to remove its disulfide bonds abolished activity (data not shown). We instead searched for peroxidases that are naturally active in reducing environments. Ascorbate peroxidase (APX) is a class I cytosolic plant peroxidase that lacks disulfide bonds and calcium ions[18]. At 28 kDa, APX is also ~40% smaller than HRP. However, APX has not previously been tested in mammalian cells, and its natural substrate, ascorbate, has a structure that is very different from DAB (**Fig. 1a**). Furthermore, wild-type (WT) APX is a constitutive homodimer[19], which is problematic because oligomeric tags can perturb a protein's natural localization and function[20].

We first tested expression and activity of WT APX, using immunostaining and the fluorogenic peroxidase substrate Amplex UltraRed, in three cellular compartments: the cytosol, mitochondrial matrix and endoplasmic reticulum (ER). For comparison, we tested HRP in the same locations. APX was strongly expressed and active in all compartments, whereas genetically targeted HRP was active only in the ER, as expected (**Supplementary Fig. 1**).

We next engineered a monomeric APX. Guided by the crystal structure (PDB ID 1APX[18]) and building upon an earlier mutagenesis study[19], we individually mutated negatively charged or neutral residues at the dimer interface to lysine to introduce repulsive interactions (**Fig. 1b**). We also tested three mutants (K14D, K31S and A233D) on the basis of sequence alignment to an isoform of maize APX that was reported to be monomeric[21]. Gel filtration chromatography was used to assess oligomerization (**Fig. 1c** and **Supplementary Fig. 2**). Five mutants were considerably more monomeric than the WT, but they all displayed weak dimerization, so we generated double and triple mutants using permutations of the five promising single mutations. A double mutant containing K14D and E112K (mAPX, for monomeric APX) exhibited the most monomericity while still being strongly expressed in *Escherichia coli* and forming minimal high molecular weight aggregates.

[1]Department of Chemistry, Massachusetts Institute of Technology, Cambridge, Massachusetts, USA. [2]National Center for Microscopy and Imaging Research, Center for Research on Biological Systems, University of California at San Diego, La Jolla, California, USA. [3]Departments of Systems Biology and Medicine, Harvard Medical School and Massachusetts General Hospital, Boston, Massachusetts, USA. [4]Broad Institute, Cambridge, Massachusetts, USA. [5]Departments of Molecular Biology and Biochemistry, Chemistry, and Pharmaceutical Sciences, University of California, Irvine, California, USA. [6]Department of Neurosciences, University of California at San Diego, La Jolla, California, USA. Correspondence should be addressed to A.Y.T. (ating@mit.edu).

Received 29 June; accepted 29 August; published online 21 October 2012; doi:10.1038/nbt.2375

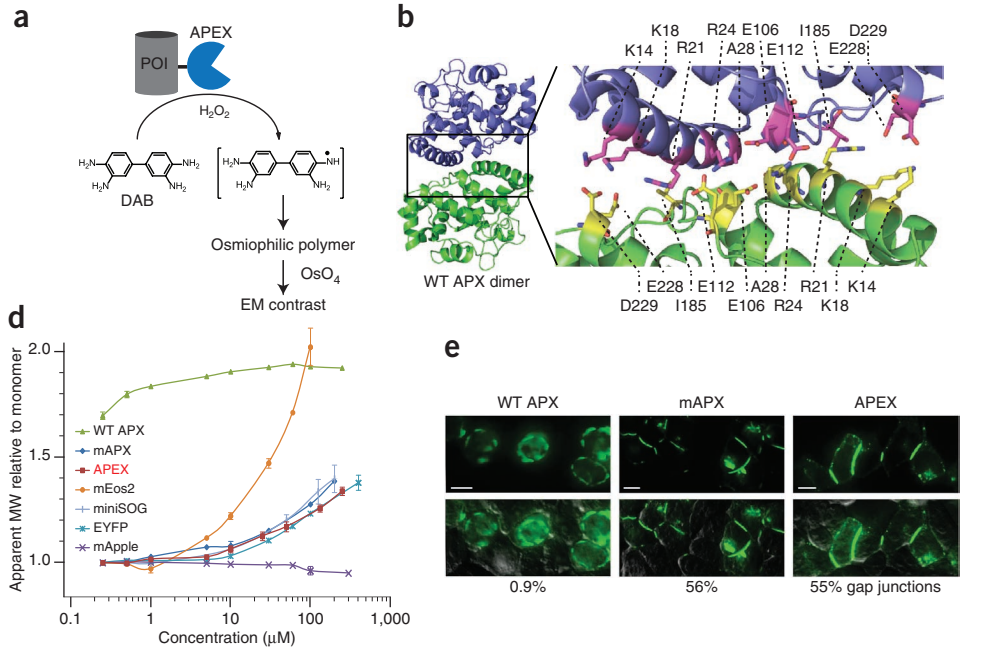

APX mutant (10 μM)	MW_{app} (kDa)	% High MW aggr. (%)
WT pAPX	56	0
K31S	56	0
A233D	58	0
I185K	42	1
K14D	39	1
A28K	37	15
E112K	36	1
E228K	34	2
D229K	34	3
A28K, E112K	34	11
K14D, D229K	34	4
K14D, E228K	33	6
E112K, E228K	33	6
K14D, E112K (mAPX)	33	4
E112K, D229K	32	6
A28K, E112K, D229K	33	25
K14D, E112K, D229K	33	8
K14D, E112K, E228K	33	4
A28K, E112K, E228K	32	9

Figure 1 EM reporter scheme and characterization of APEX oligomerization state. (**a**) The APEX reporter, a monomeric and activity-enhanced mutant of pea APX, can be genetically fused to any cellular protein of interest (POI). After expression in live cells, the cells are fixed, and a solution of diaminobenzidine (DAB) is overlaid. Upon addition of H_2O_2, APEX, which retains activity in fixative, catalyzes the oxidative polymerization of DAB to generate a cross-linked and locally deposited precipitate. Subsequent staining of the DAB polymer with electron-dense OsO_4 generates EM contrast. (**b**) Mutations were introduced at the dimer interface of wild-type (WT) APX. (**c**) Gel filtration chromatography of APX mutants. The calculated molecular weight (MW) of WT APX is 28 kDa. As expected, WT APX runs as a dimer (apparent MW 56 kDa). Some mutants also formed higher molecular weight aggregates (MW_{app} >200 kDa), which may indicate instability. The K14D, E112K double mutant (mAPX, in red) was selected for further characterization. (**d**) Gel filtration analysis of mAPX, WT APX and APEX at concentrations ranging from 250 nM to 250 μM. Dimerization of mAPX and APEX is not detected at <10 μM, but some dimerization is seen at concentrations >50 μM. For comparison, similar analyses were done under identical conditions for the fluorescent protein markers mEos2, EYFP and mApple, as well as miniSOG[2]. Error bars, mean ± s.d. of 2–3 independent measurements. For data points with s.d. values smaller than the height of the marker, no error bars are shown. (**e**) Imaging WT APX, mAPX and APEX fusions to Cx43-GFP (C-terminal fusions) in live HEK293T cells. Top row, GFP fluorescence (not normalized); bottom row, GFP overlay onto the DIC image. Gap junctions were easily detected for mAPX and APEX fusions (56% and 55% of contact sites between neighboring transfected cells contained GFP-labeled gap junctions, respectively), but not for the WT APX fusion (0.9%), which predominantly displayed fluorescence trapped in the secretory pathway. Scale bars, 10 μm.

We compared the oligomerization of mAPX to that of WT APX, miniSOG and several fluorescent proteins (mApple, EYFP and mEos2) across a range of concentrations (**Fig. 1d**). Each of the proteins was produced in *E. coli* and purified using a His_6-tag. mAPX was not as monomeric as mApple, but it was similar to EYFP and much more monomeric than either WT APX or mEos2 (ref 20). We fused both mAPX and WT APX to connexin43 (Cx43), a membrane protein that is sensitive to oligomeric tags (**Fig. 1e**)[20,22]. Whereas Cx43-WT APX was abnormally retained inside cells, both Cx43-mAPX and Cx43-GFP-mAPX localized properly to gap junctions, indicating that despite its weak residual dimerization at high concentrations, mAPX did not disrupt Cx43 trafficking.

We compared the activity of WT APX and mAPX in mammalian cells. mAPX and WT APX were equally active *in vitro* and similarly active in some cellular contexts, such as the mitochondrial matrix, which houses the last step of heme biosynthesis (**Fig. 2**). However, when fused to a nuclear export sequence (NES) and thereby expressed throughout the cytosol, mAPX was much less active than WT APX toward both DAB (**Fig. 2**) and Amplex UltraRed (**Supplementary Fig. 3a**,**b**). Culturing the cells with heme after transfection substantially boosted the activity of mAPX-NES. We reasoned that the poor activity of mAPX-NES is likely due to less efficient heme incorporation in the cellular context, which is perhaps a result of decreased thermal stability and lower melting temperature associated with monomerization[19].

To improve the performance of mAPX in mammalian cells, we engineered a monomeric APX with improved activity toward DAB in the hope that faster kinetics could compensate for diminished heme binding. We compared the substrate binding site of APX to that of HRP, which has faster kinetics and broader aromatic substrate tolerance[23]. To make APX more like HRP, we designed seven mutants of APX that incorporated mostly aromatic residues into the active site (**Fig. 2a**). We employed a colorimetric assay using guaiacol, a prototypical aromatic peroxidase substrate, to determine Michaelis-Menten kinetic parameters[24] (**Fig. 2b** and **Supplementary Fig. 4**). All of the mutations improved APX activity, with the most promising mutant showing >25-fold enhancement over WT APX in terms of k_{cat}/K_M. The most HRP-like mutant (containing W41F, G69F, D133A, T135F and K136F) was also the most active, validating our engineering approach.

To generate a monomeric APX with improved activity, we added the two mAPX mutations (K14D and E112K) to each of our activity-enhanced mutants. The monomerized versions of some activity-enhanced mutants performed poorly in several cellular contexts (**Supplementary Fig. 5**), but $mAPX^{W41F}$ was strongly expressed in *E. coli*, displayed minimal high molecular weight (MW) aggregation and localized similarly to mAPX in cells. We therefore selected $mAPX^{W41F}$(containing K14D, E112K and W41F), which we call APEX (for enhanced APX), as our optimized reporter for subsequent

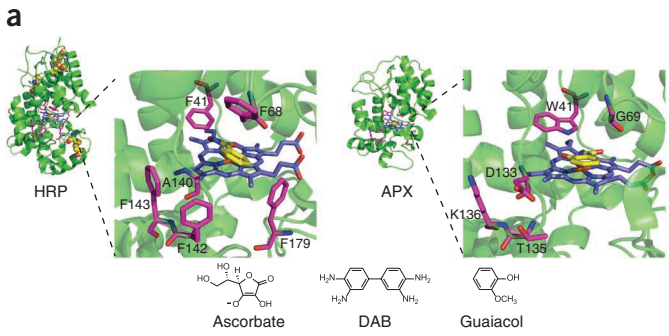

b

Enzyme	k_{cat} (s^{-1})	K_M (mM)	k_{cat}/K_M ($M^{-1}s^{-1}$)	k_{cat}/K_M rel. to WT
WT APX	41 ± 5	13.0 ± 0.8	3.2×10^3	1.0
HRP	370 ± 30	2.7 ± 0.7	1.4×10^5	43.3
W41F	109 ± 8	4.2 ± 0.9	2.6×10^4	8.2
G69F	102 ± 2	23.2 ± 0.3	4.4×10^3	1.4
FFA*	44 ± 6	3.1 ± 0.8	1.4×10^4	4.5
W41F + FFA*	65 ± 2	1.2 ± 0.2	5.4×10^4	17.1
G69F + FFA*	97 ± 8	7.6 ± 0.7	1.3×10^4	4.0
W41F + G69F	100 ± 10	2.6 ± 0.3	3.9×10^4	12.1
W41F + G69F + FFA*	106 ± 6	1.2 ± 0.1	8.8×10^4	27.9
K14D, E112K (mAPX)	60 ± 10	13.0 ± 1.0	4.6×10^3	1.5
mAPX + W41F + FFA*	79 ± 8	1.5 ± 0.5	5.3×10^4	16.6
mAPX + W41F (APEX)	111 ± 1	4.3 ± 0.2	2.6×10^4	8.1

*FFA = D133A/T135F/K136F

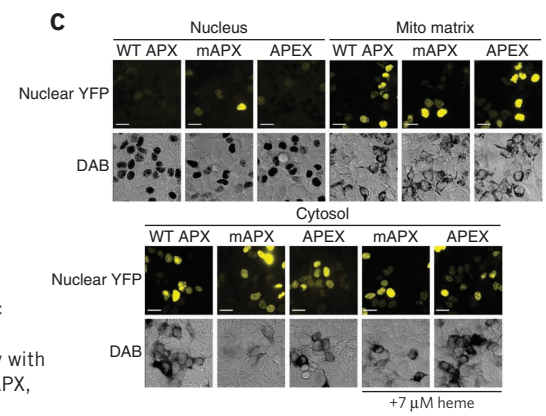

Figure 2 Active-site engineering to boost the activity of APEX. (**a**) Active sites of WT HRP and WT APX (from PDB IDs 1H5A[29] and 1VOH[30], respectively). The heme cofactor is shown in blue. The co-crystallized substrate analogs (benzohydroxamic acid for HRP and salicylhydroxamic acid for APX) are shown in yellow. The HRP active site is lined with aromatic side chains, shown in purple, whereas the APX active site has only a single tryptophan at position 41. In the full HRP structure at left, the four disulfide bonds are rendered in space-filling yellow. WT APX lacks disulfide bonds. Chemical structures of ascorbate (the natural substrate of APX), DAB (the desired substrate for EM applications) and guaiacol (a model aromatic substrate used for kinetic analysis) are shown below. (**b**) Kinetic constants of APX mutants engineered to resemble HRP. k_{cat} and K_M values were measured using a spectrophotometric assay with guaiacol as substrate. (**c**) DAB polymerization activities of WT APX, mAPX and APEX expressed in various cellular compartments. HEK293T cells were transfected with the indicated constructs, incubated with or without exogenous heme, fixed, reacted with DAB, then imaged. The top row shows fluorescence of a co-transfected nuclear YFP marker. The bottom row shows the brightfield image. DAB polymer appears dark because it absorbs light throughout the visible spectrum. For nuclear-localized constructs, DAB stain blots out the nuclear YFP fluorescence, so bright YFP fluorescence indicates poor APX activity. Scale bars, 25 μm. (**d**) The graph on the right quantifies the data for cytosolic constructs. For each condition, the mean fraction of transmitted light absorbed was calculated for >60 transfected cells, then averaged together. WT APX is the most active toward DAB in cells, followed by APEX and then mAPX. For all three constructs, heme addition boosts activity.

experiments. Notably, APEX-NES gave markedly stronger staining in cells than mAPX-NES, using both DAB (**Fig. 2c**) and Amplex UltraRed (**Supplementary Fig. 3**) as substrates. APEX is as monomeric as mAPX *in vitro* (**Fig. 1d**) and localizes properly as a fusion to Cx43, both alone and in tandem with GFP (**Fig. 1e**).

We proceeded to test the utility of APEX for EM imaging in mammalian cells. We first used APEX to stain two cellular compartments with distinct EM signatures: the mitochondrial matrix and the ER lumen. Mitochondria expressing APEX showed strong contrast and well-defined cristae structures relative to nonexpressing mitochondria (**Fig. 3a**). When localized to the ER lumen, APEX provided dense staining throughout the ER tubular network (**Fig. 3a**). By comparison, the ER lumen of untransfected cells gave weak contrast.

We next imaged APEX fused to three mammalian proteins by EM: histone 2B (H2B), vimentin and Cx43. APEX-H2B revealed detailed chromatin structures, both along the nuclear envelope and on the periphery of nucleoli (**Fig. 3a**). These features were not discernible in untransfected cells. APEX-H2B was properly incorporated into chromatin throughout all stages of mitosis (**Fig. 3a** and **Supplementary Fig. 6**), demonstrating that the weak dimerization of APEX is not perturbing in this context. Vimentin-APEX highlighted intermediate filaments throughout the cell, and subfilamentous repeating densities could be discerned (**Fig. 3a**), underscoring the excellent contrast and high resolution afforded by APEX. Cx43-GFP-APEX gave high-resolution images of gap junction plaques, revealed by both thin sections and electron tomography (**Fig. 3a** and **Supplementary Movie 1**). In some cases, gap junction plaques were closely apposed to tubular segments of ER membrane[25], but the DAB reaction product spread minimally even in the absence of membrane enclosure (**Fig. 3a**).

We used Cx43-GFP-APEX for correlated light microscopy (LM) and EM[9] by imaging GFP fluorescence in fixed cells, followed by DAB deposition and EM processing (**Fig. 3a**). Similar constructs using mCherry instead of GFP, in two different orientations, also formed gap junctions and gave bright fluorescence and strong DAB staining (**Supplementary Fig. 7**).

Because APEX remains active after membrane-preserving cell fixation and generates a minimally diffusive reaction product that does not cross membranes, we hypothesized that APEX could be useful for determining the topology of membrane proteins. The mitochondrial calcium uniporter (MCU) is a recently discovered protein channel responsible for calcium uptake into mitochondria[3,4]. Each MCU subunit contains two transmembrane segments that span the inner mitochondrial membrane. Results from a previous study[3] that used a protease accessibility assay on purified mitochondria suggested that both the N and C termini of MCU protrude into the mitochondrial matrix. In contrast, another study[4] reported the opposite topology, with both the N and C termini facing the intermembrane space (**Fig. 3b**). To resolve this discrepancy, we constructed N- and C-terminal fusions of APEX to MCU, stained samples with DAB and imaged them by EM. Consistent with the model in which both termini face the mitochondrial matrix[3], both constructs gave clear EM staining in the matrix, but not the intermembrane space (**Fig. 3c** and **Supplementary Fig. 8**). Separate controls showed that APEX is active in the intermembrane space (**Supplementary Fig. 8**).

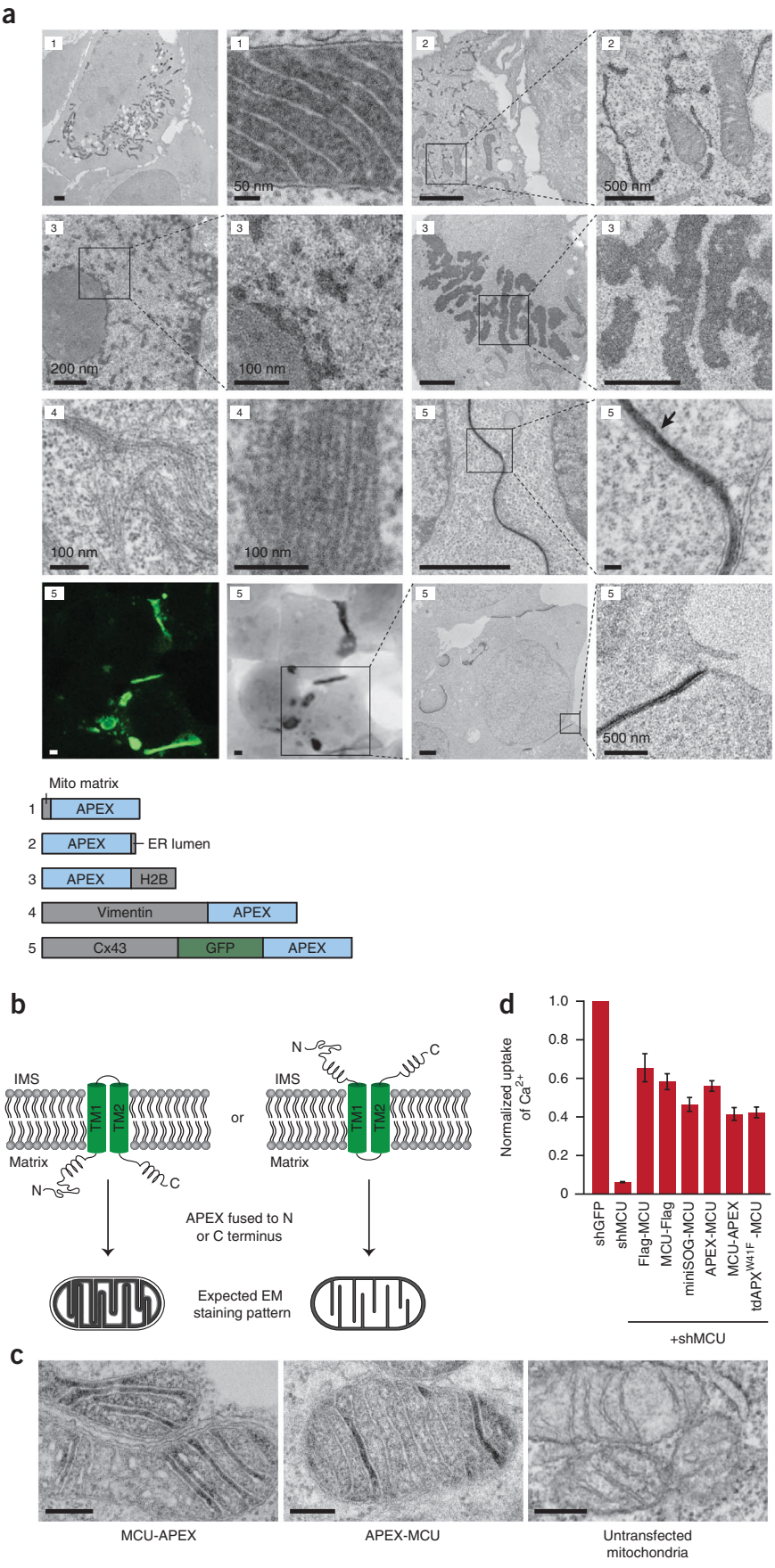

Figure 3 EM imaging of cellular proteins and organelles with APEX. (**a**) EM images of the genetic constructs shown below. Additional EM images are shown in **Supplementary Figure 6**. (1) (*left*) Low magnification image of a COS-7 cell expressing APEX in the mitochondrial matrix. Compared to neighboring untransfected cells, the APEX-expressing mitochondria give much stronger contrast. (*right*) High magnification image of a single transfected mitochondrion. (2) COS-7 cell expressing endoplasmic reticulum-targeted APEX-KDEL. (3) COS-7 cells expressing APEX fusion to histone 2B. (*two left panels*) The zoom shows chromatin detail at the border of the nucleolus. (*two right panels*) COS-7 cell in metaphase of mitosis. Zoom shows chromosome detail. (4) Vimentin intermediate filaments in a COS-7 cell. APEX enables visualization of individual filaments, and a bead-like pattern with ~20 nm repeat spacing is apparent[31]. (5) (*top two panels*) Connexin gap junction between two transfected HEK293T cells. The zoom illustrates minimal spread of the DAB reaction product, even in the absence of membrane enclosure (arrow). (*bottom four panels*) Correlated LM and EM of Cx43-GFP-APEX. Panels show (from left to right): fluorescence image before DAB stain, transmitted light image after DAB stain, low magnification EM image, and high magnification EM image. Scale bars not labeled are 2 µm; all others as indicated. (**b**) Cartoon presenting the two topology models for the mitochondrial calcium uniporter (MCU) and the predicted EM staining patterns for each model when APEX is fused to either the N or C terminus of MCU. (**c**) EM images showing the DAB staining pattern for MCU-APEX (C-terminal fusion), APEX-MCU (N-terminal fusion) and untransfected mitochondria in COS-7 cells. Both MCU-APEX and APEX-MCU give clear staining in the mitochondrial matrix, whereas the intermembrane space (IMS) is light. In this experiment, the C32A mutant of APEX was used to eliminate the possibility of disulfide bond formation, but when APEX was used without the C32A mutation, identical results were obtained (data not shown). Additional fields of view for MCU fusion constructs are presented in **Supplementary Figure 8**. Scale bars, 200 nm. (**d**) MCU fusions to APEX are functional. Stable HeLa cells with endogenous MCU replaced by the recombinant MCU constructs shown were prepared by lentiviral infection followed by selection in geneticin. MCU-mediated calcium uptake into mitochondria was measured in these cells using Oregon Green Bapta 6F fluorescence. Error bars show the s.d. from 4–6 independent measurements. shMCU refers to control cells lacking MCU (endogenous or recombinant). shGFP refers to control cells expressing endogenous MCU.

Notably, the matrix stain was strongest for both constructs at sites where cristae were closely stacked (within ~25 nm). To investigate whether this localization was an artifact

of APEX dimerization at high concentrations, we repeated the experiment using a tandem dimer of APX^{W41F} ($tdAPX^{W41F}$; description and characterization in **Supplementary Fig. 9**) as well as miniSOG in place of APEX. Identical EM staining patterns were obtained for all constructs after transient expression (**Supplementary Fig. 8**), although we still cannot rule out artifactual dimerization because miniSOG, like APEX, shows weak oligomerization at concentrations above ~20 µM (**Fig. 1d**). In a functional assay for Ca^{2+} uptake, all fusions of MCU to APEX, $tdAPX^{W41F}$ and miniSOG performed similarly to MCU appended to a small Flag epitope tag (**Fig. 3d**), indicating that none of these tags perturb function. The MCU topology revealed by APEX EM imaging has implications for MCU interaction partners and regulatory proteins, as it is now clear that most of the soluble portions of the protein reside in the matrix, rather than the intermembrane space.

We have developed APEX, an engineered variant of APX that is monomeric, can be targeted through transfection and provides strong EM contrast in all cellular compartments thus far tested, including the cytosol, where HRP is inactive as a genetic tag. Although HRP-antibody conjugates provide sensitive EM staining of cytosolic targets, the permeablizing reagents required for immunostaining irreversibly damage cellular ultrastructure and allow the DAB reaction product to spread. In contrast, cells expressing APEX can be strongly fixed with 2% glutaraldehyde in the absence of detergent, and the reaction product is generated at 4 °C, enabling optimal preservation of ultrastructure and tight localization of the EM stain.

The APEX staining protocol is straightforward, requiring only the addition of DAB and H_2O_2. Photosensitizers such as miniSOG require light, which limits their utility in complex tissues and whole organisms, whereas APEX should be fully applicable for large-scale EM of such specimens. Additionally, because APEX fusions provide a high-resolution reaction product in three dimensions, they are directly applicable to electron tomography (as demonstrated here), serial section analyses and serial blockface scanning EM. MiniSOG has two advantages over APEX: it is smaller (12 kDa versus 28 kDa) and possesses intrinsic fluorescence, which facilitates correlated LM and EM. However, miniSOG's fluorescence is weak, and correlated imaging is best done with miniSOG-fluorescent protein fusions[26]. Here we show that APEX also tolerates fusion to fluorescent proteins on either terminus, making correlated LM and EM straightforward. Because the APEX reaction conditions are orthogonal to miniSOG reaction conditions, it may be possible to use the two tags in combination to generate differentiable depositions of DAB for 'two-color' EM.

WT APX is a strong homodimer, but we have engineered APEX to be predominantly monomeric. APEX still shows residual dimerization at high concentrations, similar to EYFP and miniSOG. Despite its weak dimerization, APEX localizes properly as a fusion to numerous proteins that are sensitive to oligomerization. We did observe perturbation of ER structure when APEX was overexpressed on the ER membrane facing the cytosol (data not shown), similar to observations published for EGFP constructs[27]. To avoid dimerization artifacts, we recommend expressing APEX at the minimum level required to obtain EM contrast.

One potential limitation of APEX is its requirement for heme. In many cell types and compartments, the endogenous heme available is likely sufficient to confer high APEX activity; all images in this work, except those in **Figure 2c** where indicated, were acquired without exogenous heme supplied. In heme-poor environments, however, such as the cytosol of some cell types, the activity of APEX toward DAB may be insufficient for EM, perhaps a result of diminished heme binding resulting from decreased stability[19]. In these cases, we recommend using APX^{W41F} instead of APEX if a dimeric tag can be tolerated, or using the tandem dimer $tdAPX^{W41F}$ if a larger tag size can be tolerated, or supplementing the cell media with purified heme before fixation to increase the heme occupancy of APEX.

Beyond EM, APEX should have utility for a variety of other imaging and biotechnological applications, such as those for which HRP is currently used[28]. For example, the activity of APEX toward numerous aromatic substrates (DAB, Amplex Red and guaiacol are illustrated here) provides the opportunity not only for EM contrast, but also for colorimetric, fluorescent and chemiluminescent readouts.

METHODS

Methods and any associated references are available in the online version of the paper.

Note: Supplementary information is available in the online version of the paper.

ACKNOWLEDGMENTS

We thank A. Keating for use of her gel filtration chromatography system and A. Thor, A. Cone and M. Terada for assistance with electron tomography. The IMS-APEX EM data were obtained by H.-W. Rhee, P. Zou, J.D.M. and E.Vasile (Microscopy and Imaging Core Facility, Koch Institute at MIT). C. Uttamapinant (MIT) and H. Fraser (Stanford) provided helpful feedback on the manuscript. Funding was provided by US National Institutes of Health grants DP1 OD003961 (A.Y.T.), P41RR004050 (M.H.E.), P41GM103412 (M.H.E.), GM065937 (G.E.S.), GM072881 (G.E.S.), GM077465 (V.K.M.) and GM42614 (T.L.P.). J.D.M. was supported by a National Science Foundation Graduate Research Fellowship and a National Defense Science and Engineering Graduate Fellowship.

AUTHORS CONTRIBUTIONS

J.D.M. and A.Y.T. designed the research, analyzed the data and wrote the paper. All authors edited the paper. M.H.E. and G.E.S. oversaw EM experiments and analyzed the results. T.L.P. provided guidance on peroxidases and peroxidase assays. J.D.M. and T.J.D. performed EM sample preparation and imaging. Y.S. and V.K.M. performed calcium uptake assays and prepared MCU stable cells. J.D.M. performed all other experiments.

COMPETING FINANCIAL INTERESTS

The authors declare competing financial interests: details are available in the online version of the paper.

Published online at http://www.nature.com/doifinder/10.1038/nbt.2375.
Reprints and permissions information is available online at http://www.nature.com/reprints/index.html.

1. Hopkins, C., Gibson, A., Stinchcombe, J. & Futter, C. Chimeric molecules employing horseradish peroxidase as reporter enzyme for protein localization in the electron microscope. *Methods Enzymol.* **327**, 35–45 (2000).
2. Shu, X. *et al.* A genetically encoded tag for correlated light and electron microscopy of intact cells, tissues, and organisms. *PLoS Biol.* **9**, e1001041 (2011).
3. Baughman, J.M. *et al.* Integrative genomics identifies MCU as an essential component of the mitochondrial calcium uniporter. *Nature* **476**, 341–345 (2011).
4. De Stefani, D., Raffaello, A., Teardo, E., Szabo, I. & Rizzuto, R. A forty-kilodalton protein of the inner membrane is the mitochondrial calcium uniporter. *Nature* **476**, 336–340 (2011).
5. De Mey, J., Moeremans, M., Geuens, G., Nuydens, R. & De Brabander, M. High resolution light and electron microscopic localization of tubulin with the IGS (immuno gold staining) method. *Cell Biol. Int. Rep.* **5**, 889–899 (1981).
6. Giepmans, B.N.G., Deerinck, T.J., Smarr, B.L., Jones, Y.Z. & Ellisman, M.H. Correlated light and electron microscopic imaging of multiple endogenous proteins using Quantum dots. *Nat. Methods* **2**, 743–749 (2005).
7. Henderson, D. & Weber, K. Three-dimensional organization of microfilaments and microtubules in the cytoskeleton: Immunoperoxidase labelling and stereo-electron microscopy of detergent-extracted cells. *Exp. Cell Res.* **124**, 301–316 (1979).
8. Deerinck, T.J. *et al.* Fluorescence photooxidation with eosin: a method for high resolution immunolocalization and in situ hybridization detection for light and electron microscopy. *J. Cell Biol.* **126**, 901–910 (1994).
9. Ellisman, M.H., Deerinck, T.J., Shu, X. & Sosinsky, G.E. Picking faces out of a crowd: genetic labels for identification of proteins in correlated light and electron microscopy imaging. *Methods Cell Biol.* **111** 139–155 (2012).

10. Schnell, U., Dijk, F., Sjollema, K.A. & Giepmans, B.N.G. Immunolabeling artifacts and the need for live-cell imaging. *Nat. Methods* **9**, 152–158 (2012).
11. Tokuyasu, K.T. Application of cryoultramicrotomy to immunocytochemistry. *J. Microsc.* **143**, 139–149 (1986).
12. Porstmann, B., Porstmann, T., Nugel, E. & Evers, U. Which of the commonly used marker enzymes gives the best results in colorimetric and fluorimetric enzyme immunoassays: Horseradish peroxidase, alkaline phosphatase or [beta]-galactosidase? *J. Immunol. Methods* **79**, 27–37 (1985).
13. Connolly, C.N., Futter, C.E., Gibson, A., Hopkins, C.R. & Cutler, D.F. Transport into and out of the Golgi complex studied by transfecting cells with cDNAs encoding horseradish peroxidase. *J. Cell Biol.* **127**, 641–652 (1994).
14. Li, J., Wang, Y., Chiu, S.-L. & Cline, H. Membrane targeted horseradish peroxidase as a marker for correlative fluorescence and electron microscopy studies. *Front. Neural Circuits* **4**, 6 (2010).
15. Gaietta, G. *et al.* Multicolor and electron microscopic imaging of connexin trafficking. *Science* **296**, 503–507 (2002).
16. Uttamapinant, C. *et al.* A fluorophore ligase for site-specific protein labeling inside living cells. *Proc. Natl. Acad. Sci. USA* **107**, 10914–10919 (2010).
17. Tsien, R. Imagining imaging's future. *Nat. Rev. Mol. Cell Biol.* **4**, SS16–SS21 (2003).
18. Patterson, W.R. & Poulos, T.L. Crystal structure of recombinant pea cytosolic ascorbate peroxidase. *Biochemistry* **34**, 4331–4341 (1995).
19. Mandelman, D., Li, H., Poulos, T.L. & Schwarz, F.P. The role of quaternary interactions on the stability and activity of ascorbate peroxidase. *Protein Sci.* **7**, 2089–2098 (1998).
20. McKinney, S.A., Murphy, C.S., Hazelwood, K.L., Davidson, M.W. & Looger, L.L. A bright and photostable photoconvertible fluorescent protein. *Nat. Methods* **6**, 131–133 (2009).
21. Koshiba, T. Cytosolic ascorbate peroxidase in seedlings and leaves of maize (*Zea mays*). *Plant Cell Physiol.* **34**, 713–721 (1993).
22. Lauf, U., Lopez, P. & Falk, M.M. Expression of fluorescently tagged connexins: a novel approach to rescue function of oligomeric DsRed-tagged proteins. *FEBS Lett.* **498**, 11–15 (2001).
23. Henriksen, A., Smith, A.T. & Gajhede, M. The structures of the horseradish peroxidase C-ferulic acid complex and the ternary complex with cyanide suggest how peroxidases oxidize small phenolic substrates. *J. Biol. Chem.* **274**, 35005–35011 (1999).
24. Lad, L., Mewies, M. & Raven, E.L. Substrate binding and catalytic mechanism in ascorbate peroxidase: evidence for two ascorbate binding sites. *Biochemistry* **41**, 13774–13781 (2002).
25. Sosinsky, G.E. *et al.* Tetracysteine genetic tags complexed with biarsenical ligands as a tool for investigating gap junction structure and dynamics. *Cell Commun. Adhes.* **10**, 181–186 (2003).
26. Qi, Y.B., Garren, E.J., Shu, X., Tsien, R.Y. & Jin, Y. Photo-inducible cell ablation in *Caenorhabditis elegans* using the genetically encoded singlet oxygen generating protein miniSOG. *Proc. Natl. Acad. Sci. USA* **109**, 7499–7504 (2012).
27. Costantini, L.M., Fossati, M., Francolini, M. & Snapp, E.L. Assessing the tendency of fluorescent proteins to oligomerize under physiologic conditions. *Traffic* **13**, 643–649 (2012).
28. Ryan, B., Carolan, N. & Ó'Fágáin, C. Horseradish and soybean peroxidases: comparable tools for alternative niches? *Trends Biotechnol.* **24**, 355–363 (2006).
29. Berglund, G. *et al.* The catalytic pathway of horseradish peroxidase at high resolution. *Nature* **417**, 463–468 (2002).
30. Sharp, K.H., Moody, P.C.E., Brown, K.A. & Raven, E.L. Crystal structure of the ascorbate peroxidase salicylhydroxamic acid complex. *Biochemistry* **43**, 8644–8651 (2004).
31. Kirmse, R., Bouchet-Marquis, C.d., Page, C., Hoenger, A. & Thomas,, M.R. Three-dimensional cryo-electron microscopy on intermediate filaments. in *Methods in Cell Biology*, Vol. 96 (eds. Müller-Reichert, T. & Verkade, P.) 565–589 (Academic Press, 2010).

ONLINE METHODS

Cloning and mutagenesis. The pTRC99A bacterial expression vector encoding pea cytosolic APX with a His_6-tag appended to its N terminus has been described previously[32]. Mutants of APX were generated using QuikChange mutagenesis (Stratagene) or overlap extension PCR[33]. Some mutants were subcloned into the pET21a bacterial expression vector (EMD Chemicals) between the NdeI and XhoI restriction sites, which enabled higher protein yield than pTRC. Fusions of APX to mammalian proteins and localization signals were generated using standard restriction cloning methods. **Supplementary Table 1** presents an overview of all mammalian expression constructs used in this study. For most of these mammalian expression constructs, the original pea APX gene was used. For some constructs, however, we used a pea APX gene with humanized codons, synthesized by GenScript. We avoided the use of HA epitope tags for immunofluorescence detection because the HA tag, being tyrosine rich, is oxidatively damaged by APX in the presence of H_2O_2.

Gel filtration chromatography. Purified APX, miniSOG or fluorescent proteins were diluted to the desired concentrations using chilled (4 °C) PBS (137 mM NaCl, 2.7 mM KCl, 10 mM Na_2HPO_4, 2.0 mM KH_2PO_4, pH 7.4) and then allowed to incubate at room temperature for 30 min to overnight. APX was not prone to aggregation on the timescale of hours at room temperature. Samples (100 µL) were run on a Waters HPLC system over a Superdex 75 10/300 column (GE Healthcare) that had been pre-equilibrated in PBS, pH 7.4. Samples were run isocratically at room temperature in PBS at a flow rate of 0.5 mL/min. Elution of APX was monitored at 280 nm and 405 nm (heme absorbance). Empower software (Waters) was used for analysis of elution profiles. Apparent MWs were determined by referencing low molecular weight standards (GE) (**Supplementary Fig. 2**). For proteins that exhibited no significant change in apparent MW between 0.25 and 1 µM, the apparent MW of the monomer was estimated to be equal to the apparent MW at 0.25 µM. This estimation was applied for all proteins in **Figure 1d** except for WT APX, which was predominantly dimeric at 0.25 µM. The apparent MW of the monomer for WT APX was assumed to be equal to the apparent MW of mAPX at 0.25 µM.

Guaiacol activity assay. We attempted to establish an assay to monitor the APX-catalyzed polymerization of DAB *in vitro*, but could not determine the kinetic parameters for this complex process. Amplex UltraRed was also not used for kinetic measurements as the K_M of APX toward aromatic substrates is typically between 1 and 10 mM, and solutions of Amplex UltraRed cannot be economically prepared at these high concentrations. We used guaiacol as the substrate to measure peroxidase kinetics instead. Good activity toward guaiacol generally correlated well with robust polymerization of DAB *in vitro* (data not shown). Guaiacol assays were done on a Nanodrop 2000c UV-vis spectrophotometer (Thermo Scientific) using its cuvette reader. HRP (Sigma) was prepared as a 10 µM stock in PBS, flash frozen and stored at −80 °C, and thawed immediately before use. Guaiacol peroxidase activity was measured according to a published protocol[24]. Briefly, guaiacol (Sigma) was diluted in room temperature PBS, pH 7.4, to concentrations ranging from 0.25 to 30 mM. Solutions were vortexed thoroughly to ensure the guaiacol was completely dissolved. H_2O_2 was added to a final concentration of 90 µM, followed by addition of APX to a final concentration of 20 nM. For HRP, when 90 µM H_2O_2 was used, all of the H_2O_2 was consumed so quickly that the initial rate of guaiacol turnover could not be determined on our spectrophotometer. Therefore, 10 mM H_2O_2 was used for HRP. Under these conditions, the initial rate of turnover was maintained for several seconds and could be readily determined. Oxidation to tetraguaiacol was monitored by absorbance at 470 nm ($\varepsilon_{470} = 22 \times 10^3\ M^{-1}cm^{-1}$)[24]. k_{cat} and K_M were calculated by nonlinear regression fitting to the Michaelis-Menten equation using OriginPro. All values are reported as the mean ± s.d. for 2–3 independent Michaelis-Menten fittings, with each fitting using at least five values of substrate concentration ranging between 0.25 and 30 mM.

Mammalian cell culture and transfection. HEK293T, HeLa and COS-7 cells were cultured as a monolayer in Modified Eagle's Medium (MEM, Cellgro) supplemented with 10% FBS (PAA Laboratories). Cells were maintained at 37 °C under an atmosphere of 5% CO_2. For EM imaging experiments, cells were grown on poly-D-lysine–coated glass-bottom dishes (P35GC-0-14-C, MatTek Corp.). To improve the adherence of HEK293T cells, we also pretreated the dishes pretreated with 50 µg/mL fibronectin (Millipore) for 1 h at 37 °C before cell plating. Cells were transfected at 60–90% confluence using Lipofectamine 2000 (Life Technologies), typically with 0.7 µL Lipofectamine and 100 ng plasmid per 300,000 cells. Cells were labeled and/or fixed 18–24 h after transfection. For incubation of HEK293T cells with heme (**Fig. 2c**), the media was supplemented with a heme-bovine serum albumin (BSA) complex (3 or 7 µM)[34] for 16–24 h, after which time the media was removed, cells were rinsed 1× with non-heme-containing media then processed for imaging. Note that all images, except those in **Figure 2c** where indicated, were acquired without exogenous heme supplied. APEX generally affords strong EM staining with no requirement for exogenous heme addition, so we recommend supplementing the media with heme only in cases where the DAB stain is not sufficiently strong for EM without heme addition.

DAB staining and preparation of cultured cells for EM. Transfected cells were fixed using room temperature 2% glutaraldehyde (Electron Microscopy Sciences) in buffer (100 mM sodium cacodylate with 2 mM $CaCl_2$, pH 7.4), then quickly moved to ice. Cells were kept between 0 and 4 °C for all subsequent steps until resin infiltration. After 30–60 min, cells were rinsed 5 × 2 min in chilled buffer, then treated for 5 min in buffer containing 20 mM glycine to quench unreacted glutaraldehyde, followed by 5 × 2 min rinses in chilled buffer. A freshly diluted solution of 0.5 mg/mL (1.4 mM) DAB tetrahydrochloride or the DAB free base (Sigma) dissolved in HCl was combined with 0.03% (v/v) (10 mM) H_2O_2 in chilled buffer, and the solution was added to cells for 1 to 15 min, depending on the sample. A summary of cell types and DAB reaction times is presented in **Supplementary Table 2**. The generation of reaction product could be monitored by transmitted LM. To halt the reaction, the DAB solution was removed, and cells were rinsed 5 × 2 min with chilled buffer. Post-fixation staining was performed with 2% osmium tetroxide (Electron Microscopy Sciences) for 30 min in chilled buffer. Cells were rinsed 5 × 2 min in chilled distilled water, then placed in chilled 2% aqueous uranyl acetate (Electron Microscopy Sciences) overnight. The samples were then dehydrated in a cold graded ethanol series (20%, 50%, 70%, 90%, 100%, 100%) 2 min each, rinsed once in room temperature anhydrous ethanol to avoid condensation, and infiltrated in Durcupan ACM resin (Electron Microscopy Sciences) using 1:1 (v/v) anhydrous ethanol and resin for 30 min, then 100% resin 2 × 1 h, then into fresh resin and polymerized in a vacuum oven at 60 °C for 48 h.

EM. DAB-stained areas of embedded cultured cells were identified by transmitted light, and the areas of interest were sawed out using a jeweler's saw and mounted on dummy acrylic blocks with cyanoacrylic adhesive (Krazy Glue, Elmer's Products). The coverslip was carefully removed, the block trimmed, and ultrathin (80 nm thick) sections were cut using an ultramicrotome (Leica Ultracut UTC6). Electron micrographs were recorded using a JEOL 1200 TEM operating at 80 keV.

Amplex UltraRed labeling and immunostaining. Transfected cells on glass coverslips were moved to ice, then treated with a solution of 50 µM Amplex UltraRed (Molecular Probes) with 0.02% (6.7 mM) H_2O_2 in Dulbecco's phosphate-buffered saline (DPBS). The Amplex UltraRed solution was freshly diluted from a 10 mM stock in dimethyl sulfoxide. After 5–30 min, depending on the sample, the Amplex UltraRed solution was removed and replaced with DPBS. In some cases, cells were imaged live. Strong resorufin signal was present in cells expressing APX, although the signal was not tightly localized to the site of origin. Alternatively, Amplex UltraRed-stained cells were fixed using freshly depolymerized 4% formaldehyde (Electron Microscopy Sciences) in PBS for 30 min on ice, rinsed 5 × 2 min in chilled PBS then treated with methanol for 5–10 min at −20 °C. Samples were blocked using 1% (v/v) bovine serum albumin (BSA, Fisher Scientific) in PBS at 4 °C for 30 min, then treated overnight at 4 °C with a 1:500 dilution of mouse-anti-Flag antibody (Agilent) or chicken-anti-*c*-myc antibody (Life Technologies) in PBS with 1% BSA. Cells were rinsed 4 × 5 min in PBS, then treated with a 1:750 dilution of Alexa Fluor 488 goat anti-mouse IgG or Alexa Fluor 568 goat anti-chicken IgG (Life Technologies) for 15 min at 4 °C. Cells were rinsed 4 × 5 min in PBS, then imaged by confocal microscopy.

At this point, much of the resorufin had been washed away, but the remaining label was more closely localized to the site of origin.

APX expression and purification. N-terminally His_6-tagged APX and its mutants were expressed from pET21a or pTRC expression vectors in the BL21-DE3 strain of *E. coli*. The pET21a vector gave significantly higher yield of APX, but a low percentage of heme incorporation (as determined by A_{405}/A_{280} ratio), whereas pTRC gave a lower yield of APX with a high percentage of heme incorporation. Individual colonies were amplified in 500 mL Luria Broth (LB) supplemented with 10 μg/mL ampicillin and grown to an OD_{600} of 0.6 at 37 °C. Protein expression was then induced with 420 μM isopropyl β–D-1-thiogalactopyranoside (IPTG) overnight at room temperature. Cells were harvested by centrifugation at 6,400*g* and lysed using B-PER (Bacterial Protein Extraction Reagents, Pierce) with 1 mM PMSF and protease inhibitor cocktail (Sigma). The lysates were allowed to rock at 4 °C for 30 min, then centrifuged at 11,000*g*. The supernatant was incubated with 1.5 mL Ni-NTA agarose slurry (Qiagen) for 30 min. The APX-bound resin was loaded onto an Econo-Pac column (Bio-Rad) using gravity flow at 4 °C. The resin was washed with 8 mL binding buffer (50 mM Tris-HCl, 300 mM NaCl, pH 7.8) and 8 mL washing buffer (binding buffer with 30 mM imidazole). APX was eluted in binding buffer with 200 mM imidazole and dialyzed extensively (3 × 4 L) at 4 °C in phosphate buffered saline (PBS, 137 mM NaCl, 2.7 mM KCl, 10 mM Na_2HPO_4, 2.0 mM KH_2PO_4, pH 7.4). When required, samples were concentrated using an Amicon Ultra-4 filter with Ultracel-10 membrane (Millipore). Purity was checked using SDS-PAGE (**Supplementary Fig. 2**). Protein samples were flash frozen in liquid N_2 and stored in aliquots at −80 °C.

Heme addition to purified peroxidases *in vitro*. The heme occupancy of purified APX samples was assessed using A_{403}/A_{280}, as previously described[35]. APX samples expressed from pTRC typically possessed a high degree of heme incorporation, as indicated by $A_{403}/A_{280} > 2.0$, and were therefore deemed pure[35]. In cases when A_{403}/A_{280} of an APX sample was <2.0, heme reconstitution was carried out according to a published procedure[32] with a few modifications. Note that all of the samples analyzed by gel filtration chromatography (**Fig. 1c** and **Supplementary Fig. 2**) were expressed from pTRC, allowing the reconstitution step to be bypassed. The samples used for kinetic analysis were expressed from pET21a, followed by heme reconstitution, enabling large quantities of holo enzyme to be isolated and utilized for multiple experiments. APX samples were dialyzed extensively (3 × 4 L) at 4 °C in 20 mM KPO_4, pH 7.0. To generate a heme stock, 50 mg of hemin-Cl (Sigma) was diluted in 2.0 mL of 10 mM NaOH. The mixture was thoroughly resuspended, then diluted further using 8.0 mL of 20 mM KPO_4, pH 7.0, and vortexed extensively. The mixture was centrifuged at 7,500*g* for 8 min at 4 °C to remove aggregates. The pellet was discarded, and the centrifugation was repeated. The resulting supernatant was used as the working heme stock. We added 600 μL of heme stock to 200 μL of APX (between 100 and 400 μM) in 100 μL increments over a period of 20 min. Both heme and APX samples were wrapped in foil to prevent photodamage. The heme-APX mixture was gently agitated at 4 °C for 3 h, then centrifuged at 7,500*g* for 15 min at 4 °C to remove aggregates. The supernatant was loaded onto a HiTrap DEAE Fast-flow 5 mL column (GE Healthcare) that had been pre-equilibrated with 20 mM KPO_4, pH 7.0, at 4 °C. The column was washed with 5 column volumes of 20 mM KPO_4, pH 7.0, followed by elution with 5 column volumes of 100 mM KPO_4 pH 7.0. At this ionic strength, both WT APX and mutants of APX eluted from the column, whereas excess heme remained bound. APX typically eluted over a volume of ~25 mL. Fractions containing reconstituted APX were identified by absorbance at 280 nm, then concentrated at 4 °C and exchanged into PBS buffer (3 × 4 mL) using an Amicon Ultra-4 filter with Ultracel-10 membrane (Millipore). Reconstituted APX samples with $A_{403}/A_{280} > 2.0$ were deemed pure[35], checked by 16% SDS-PAGE, and flash frozen in liquid N_2 for storage at −80 °C.

DAB photo-oxidation with miniSOG-MCU for EM. For photo-oxidation of miniSOG-MCU, cells were fixed for 30 min with 2% glutaraldehyde in 0.1 M sodium cacodylate buffer, then rinsed in the same buffer to remove unreacted glutaraldehyde. The region of interest was identified by fluorescence microscopy (Leica TCS SPE-II confocal imaging system) and an image recorded with care not to bleach the area. The cells were then placed in oxygenated DAB (0.5 mg/mL) in cacodylate buffer and the sample illuminated using a standard FITC filter set (EX470/40, DM510, BA520) with intense light from a 150W xenon lamp. Illumination was stopped as soon as a very light brown reaction product began to appear in place of the green fluorescence as monitored by transmitted light (typically 3–5 min). The samples were then rinsed in buffer, post-fixed in 1% osmium tetroxide in cacodylate buffer for 30 min, and dehydrated and embedded for EM as described above.

Generation of stable MCU cells. Stable knockdown of endogenous MCU in HeLa cells was achieved using lentiviral short hairpin (sh)RNA-expressing constructs that target the 3′ UTR of MCU (Broad RNAi Consortium ID: TRCN0000133861) as previously described[3]. shRNA that targets GFP was used as a control. Both shRNA constructs were obtained from the Broad Institute RNAi Consortium and carry a puromycin resistance gene. Cells were selected with 2 μg/ml puromycin. For rescue experiments, stable MCU knockdown cells were infected with lentiviral cDNA-expressing constructs that carry geneticin resistance, and cells were selected with 400 μg/ml of geneticin for 10 days. Expression of the recombinant MCU constructs was confirmed by Western blot analysis (data not shown).

Measurement of mitochondrial calcium uptake. The protocol has been previously described[3]. Briefly, 1 million HeLa cells were permeabilized in 150 μL of KCl buffer (125 mM KCl, 2 mM K_2HPO_4, 1 mM $MgCl_2$, 20 mM Hepes KOH, pH 7.0) with 5 mM glutamate, 5 mM malate, 1 μM Oregon Green Bapta 6F (Invitrogen cat. no. O23990) and 0.01 % (w/v) digitonin. Free calcium outside mitochondria was monitored every 0.2 s using the fluorescence of Ca^{2+}-bound Oregon Green (exc. 492/em. 517) at room temperature after injection of 50 μM $CaCl_2$. Fluorescence was recorded on a PerkinElmer Envision plate reader with FITC filters. Fluorescence intensity over 20–30 s was fit into linear graphs, the slope of the curve was calculated to find the rate of calcium uptake and each slope was normalized to the GFP control.

Fluorescence microscopy. Confocal imaging was performed with a Zeiss AxioObserver inverted microscope with 40× and 63× oil-immersion objectives, outfitted with a Yokogawa spinning disk confocal head, a Quad-band notch dichroic mirror (405/488/568/647), and 405 (diode), 491 (DPSS), 561 (DPSS) and 640 nm (diode) lasers (all 50 mW). CFP (405 laser excitation, 445/40 emission), YFP/GFP/Alexa Fluor 488 (491 laser excitation, 528/38 emission), Alexa Fluor 568/resorufin (561 laser excitation, 617/73 emission) and differential interference contrast (DIC) images were collected using Slidebook (Intelligent Imaging Innovations). All image analysis was performed in Slidebook. Fluorophore channels in each experiment were normalized to the same intensity ranges. Acquisition times ranged from 100 ms to 1 s.

Gap junction and DAB stain intensity statistics in mammalian cells. In **Figure 1e**, the numbers below the images denote the percentage of contact sites between neighboring transfected cells containing detectable gap junctions. Any cell displaying detectable GFP fluorescence was considered transfected. Contact sites between neighboring transfected cells were identified using DIC imaging. Gap junctions were identified as lines of GFP fluorescence unambiguously overlaying with the plasma membranes of two neighboring transfected cells based on DIC. In **Figure 2c**, DAB stain intensity for APX-NES variants was analyzed using Slidebook. Transfected cells were identified by nuclear YFP fluorescence. In each transfected cell, a representative DAB-stained region was encircled, and its average brightfield intensity was calculated. Background intensity, determined for each field of view by encircling a representative region in the cytosol of an untransfected cell, was subtracted out. The bar graph in **Figure 2d** represents mean data from >60 transfected cells per condition.

Electron tomography. 0.5 μm-thick sections of cells expressing Cx43-GFP-APEX were cut and imaged using a 4000 IVEM (JEOL) EM instrument operated at 400 keV. The sections were tilted and images recorded every 2° from ±60° to −60° at 40,000× magnification. The effective pixel size was 0.37 nm. A second orthogonal tilt series was recorded as well. The image stack was aligned and reconstructions were obtained using R-weighed back projection methods with the IMOD[36] or TxBr tomography package[37]. Volumes are displayed

doi:10.1038/nbt.2375

with IMOD and animations created with IMOD, IMovie, Photoshop and Quicktime Pro. Full-resolution movies are available for public downloading from the Cell Centered Database[38] with Microscopy Product ID #83884 (http://ccdb.ucsd.edu/CCDBWebSite/index.html).

32. Cheek, J., Mandelman, D., Poulos, T. & Dawson, J. A study of the K+-site mutant of ascorbate peroxidase: mutations of protein residues on the proximal side of the heme cause changes in iron ligation on the distal side. *J. Biol. Inorg. Chem.* **4**, 64–72 (1999).
33. Ho, S.N., Hunt, H.D., Horton, R.M., Pullen, J.K. & Pease, L.R. Site-directed mutagenesis by overlap extension using the polymerase chain reaction. *Gene* **77**, 51–59 (1989).
34. Richards, M.K. & Marletta, M.A. Characterization of neuronal nitric oxide synthase and a C415H mutant, purified from a baculovirus overexpression system. *Biochemistry* **33**, 14723–14732 (1994).
35. Barrows, T.P. & Poulos, T.L. Role of electrostatics and salt bridges in stabilizing the compound i radical in ascorbate peroxidase. *Biochemistry* **44**, 14062–14068 (2005).
36. Kremer, J.R., Mastronarde, D.N. & McIntosh, J.R. Computer visualization of three-dimensional image data using IMOD. *J. Struct. Biol.* **116**, 71–76 (1996).
37. Lawrence, A., Bouwer, J.C., Perkins, G. & Ellisman, M.H. Transform-based backprojection for volume reconstruction of large format electron microscope tilt series. *J. Struct. Biol.* **154**, 144–167 (2006).
38. Martone, M.E. *et al.* A cell-centered database for electron tomographic data. *J. Struct. Biol.* **138**, 145–155 (2002).